

LA-UR-11-04562

*Approved for public release;
distribution is unlimited.*

Title: MCNP6 calculations of secondary particle production in a thick Line C exit window for proton radiography (U)

Author(s): John D. Zumbro
XCP-7, Transport Applications
Los Alamos National Laboratory

Intended for: Distribution



Los Alamos National Laboratory, an affirmative action/equal opportunity employer, is operated by the Los Alamos National Security, LLC for the National Nuclear Security Administration of the U.S. Department of Energy under contract DE-AC52-06NA25396. By acceptance of this article, the publisher recognizes that the U.S. Government retains a nonexclusive, royalty-free license to publish or reproduce the published form of this contribution, or to allow others to do so, for U.S. Government purposes. Los Alamos National Laboratory requests that the publisher identify this article as work performed under the auspices of the U.S. Department of Energy. Los Alamos National Laboratory strongly supports academic freedom and a researcher's right to publish; as an institution, however, the Laboratory does not endorse the viewpoint of a publication or guarantee its technical correctness.

Los Alamos

NATIONAL LABORATORY

research note

Computation Physics Division
Transport Applications

Group XCP-7, MS F663
Los Alamos, New Mexico 87545

Fax: 505-665-2879

To/MS: Distribution

From/MS: John D. Zumbro / XCP-7, MS F663

Phone/Email: 5-1009 / zumbro@lanl.gov

Thru/MS: Avneet Sood / XCP-7, MS F663

Phone/Email: 7-2119 / sooda@lanl.gov

Symbol: XCP-7:11-011 [LA-UR-11-04562]

Date: 2 August 2011

SUBJECT: MCNP6 calculations of secondary particle production in a thick Line C exit window for proton radiography (U)

Abstract

In a recent JOWOG 32P talk (2011 May 20) results were presented for MCNP6 calculations of the production of secondary particles in an exit window used for dynamic proton radiography experiments. In this note the quantitative numbers from those calculations are presented along with a description of the model.

I. Introduction with a bit of history

The Clinton P. Anderson Meson Physics Facility at Los Alamos (LAMPF) [the facility is now call LANSCE, Los Alamos Neutron Scattering Center] was built over four decades ago to, among other things, make beams of secondary particle (specifically beams of mesons, i.e. pions and muons). This was accomplished by running the high-intensity 800-MeV proton beam from the accelerator through ‘pion’ production targets. Beams at forward angles (at 35° for EPICS [Energetic Pion Channel and Spectrometer], at 45° for LEP [Low Energy Pion], at 20° for P³ [Pion Particle Physics] and at 60° for SMC [Stopped Muon Channel]; not all that forward) were directed to secondary target area for experiments. The first two beam channels (EPICS and LEP) viewed a common 3-cm thick graphite target and the latter two channels (P³ and SMC) were designed to view a 6-cm thick graphite target.

In proton radiography the image is generated by focusing particle trajectories from an object onto an image plane with a magnetic lens at forward angles (i.e. in the range from 0 degrees to ~1 degree). The detector at the image plane, while not necessarily, has generally been an ionizing radiation-to-light converter (i.e. a fast scintillator) and a camera system is arranged to take optical pictures of this scintillator.

Because the transport of the protons through the magnetic lens is in vacuum there is a window immediately upstream of the scintillator. In the case of dynamic experiments (i.e. experiments involving the detonation of high explosives) this typical window might be 1/8" of glass followed by 1/8" of aluminum. The bottom line is that this window (1.27 cm of material) could be a particle production target at 0 degrees, and in this note the results of MCNP6 calculations looking at the production on secondary particles are presented.

MCNP6 is a developmental version¹ of MCNP which, in addition to neutrons, photons, and electrons, can transport twenty-four (24) additional particles. Particle production on nuclear targets is currently accomplished using the CEM (Cascade Exciton Model).² While trying to do transport runs (for protons, muons, pions, deuterons, tritons, ³He, and alphas) through the whole Line C proton radiography system (diffuser to image plane) it was noticed that the object to diffuser times for all particles, regardless of particle energy, was highly correlated. This indicated that the protons were producing secondary particles near the image plane, hence the study reported here.

II. The MCNP6 Model # 1

The MCNP6 model, for which results will be presented, was quite simple and a sample input is presented in Appendix I. Simply a line beam of mono-energetic protons along the z-axis (starting at -100 cm) was incident on a window as described above (1/8" of

glass followed by 1/8" of aluminum). The window extended from -0.3175-cm to 0.0-cm (SiO₂ with density 2.65 grams per cc) and from 0.0-cm to +0.3175-cm (Al with density 2.70 grams per cc); this was followed by a drift from 0.3175 cm to 100 cm in void (i.e. vacuum); from 100 cm to 100.2 cm there was LSO (Lu₂SiO₅ with density 7.36 gram per cc).

Results for various particles were tallied in fmesh (track length) tallies that were from -7 cm to +7 cm in both dimensions transverse to the z-axis and from 100.0 cm to 100.2 cm along the z-axis. There were separate fmesh tallies for protons, π^+ , π^- (charged pions), deuterons, tritons, helions (³He) and alphas. There is the possibility of other particles or recoiling nuclei but in this study we present results for only these particles.

In addition to the results for the fmesh tallies, results are also presented for a different set of fmesh tallies where an energy dependent multiplier is used for the various particle tallies. In this case the multiplier for a given particle is the dE/dx in LSO at a given energy divided by the value of dE/dx in LSO for a 1-GeV proton. It is thought that this should account for differences in a given particles ionization energy in the LSO scintillator the tallies are overlaid on. The MCNP input for these multipliers can be found in the sample input deck in Appendix I.

III. Results for Model #1

The results of the MCNP6 fmesh tallies are given in Table I as a ratio to the proton fmesh tally. These results are also plotted in Figure 1a. Table II gives (plotted in Figure 1b) the results when an energy dependent multiplier (that is different for each particle) is applied. The protons are also multiplied by an energy dependent multiplier.

Energy (MeV)	π^+	Error	π^-	Error	d	Error	t	Error	³ He	Error	α	Error
800	1.73E-03	1.85E-05	1.34E-03	1.63E-05	3.76E-03	2.73E-05	8.56E-04	1.30E-05	2.11E-04	6.46E-06	2.88E-04	7.56E-06
750	1.55E-03	1.75E-05	1.16E-03	1.52E-05	3.46E-03	2.62E-05	7.74E-04	1.24E-05	1.90E-04	6.13E-06	2.58E-04	8.35E-06
700	1.35E-03	1.63E-05	9.82E-04	1.40E-05	3.17E-03	2.51E-05	6.93E-04	1.17E-05	1.69E-04	5.79E-06	2.28E-04	6.73E-06
650	1.13E-03	1.50E-05	8.06E-04	1.26E-05	2.87E-03	2.38E-05	6.12E-04	1.10E-05	1.48E-04	5.40E-06	1.99E-04	6.3E-06
600	8.96E-04	1.33E-05	6.47E-04	1.13E-05	2.56E-03	2.30E-05	5.33E-04	1.00E-05	1.29E-04	5.10E-06	1.71E-04	5.8E-06
550	6.71E-04	1.15E-05	4.91E-04	9.88E-06	2.28E-03	2.10E-05	4.64E-04	9.59E-06	1.10E-04	4.68E-06	1.45E-04	5.4E-06
500	4.62E-04	9.58E-06	3.49E-04	8.33E-06	1.99E-03	1.99E-05	3.94E-04	8.85E-06	9.31E-05	4.30E-06	1.21E-04	4.91E-06

Table I – The values of the fmesh for the indicated particle as a ratio to the value for protons is given.

Energy (MeV)	π^+	Error	π^-	Error	d	Error	t	Error	³ He	Error	α	Error
800	2.54E-03	2.11E-05	2.03E-03	1.89E-05	4.55E-02	8.93E-05	1.57E-02	5.24E-05	1.28E-02	4.74E-05	3.15E-02	7.43E-05
750	2.27E-03	1.97E-05	1.74E-03	1.73E-05	4.11E-02	8.40E-05	1.39E-02	4.89E-05	1.14E-02	4.42E-05	2.78E-02	1.08E-04
700	1.97E-03	1.82E-05	1.45E-03	1.56E-05	3.67E-02	7.84E-05	1.22E-02	4.53E-05	9.95E-03	4.09E-05	2.42E-02	6.38E-05
650	1.71E-03	1.70E-05	1.21E-03	1.43E-05	3.33E-02	7.48E-05	1.09E-02	4.3E-05	8.82E-03	3.85E-05	2.14E-02	6.00E-05
600	1.38E-03	1.51E-05	9.70E-04	1.26E-05	2.93E-02	6.9E-05	9.34E-03	3.9E-05	7.55E-03	3.5E-05	1.82E-02	5.5E-05
550	1.04E-03	1.30E-05	7.35E-04	1.09E-05	2.54E-02	6.4E-05	7.96E-03	3.6E-05	6.35E-03	3.20E-05	1.52E-02	4.9E-05
500	7.30E-04	1.07E-05	5.21E-04	9.02E-06	2.18E-02	5.83E-05	6.61E-03	3.21E-05	5.26E-03	2.86E-05	1.25E-02	4.41E-05

Table II – The values of the fmesh for the indicated particle as a ratio to the value for protons is given. This is for the case where each tally has an energy dependent multiplier that is dE/dx over dE/dx of a 1-GeV proton. Note that these tally multipliers are different for each particle type.

One sees by comparing Figures 1 and 2 that there is other an order of magnitude increase in this signal for the case of the energy dependent multiplier. The ratios of the sums are given in Table III, and these figures are those that were presented at the recent JOWOG32P.

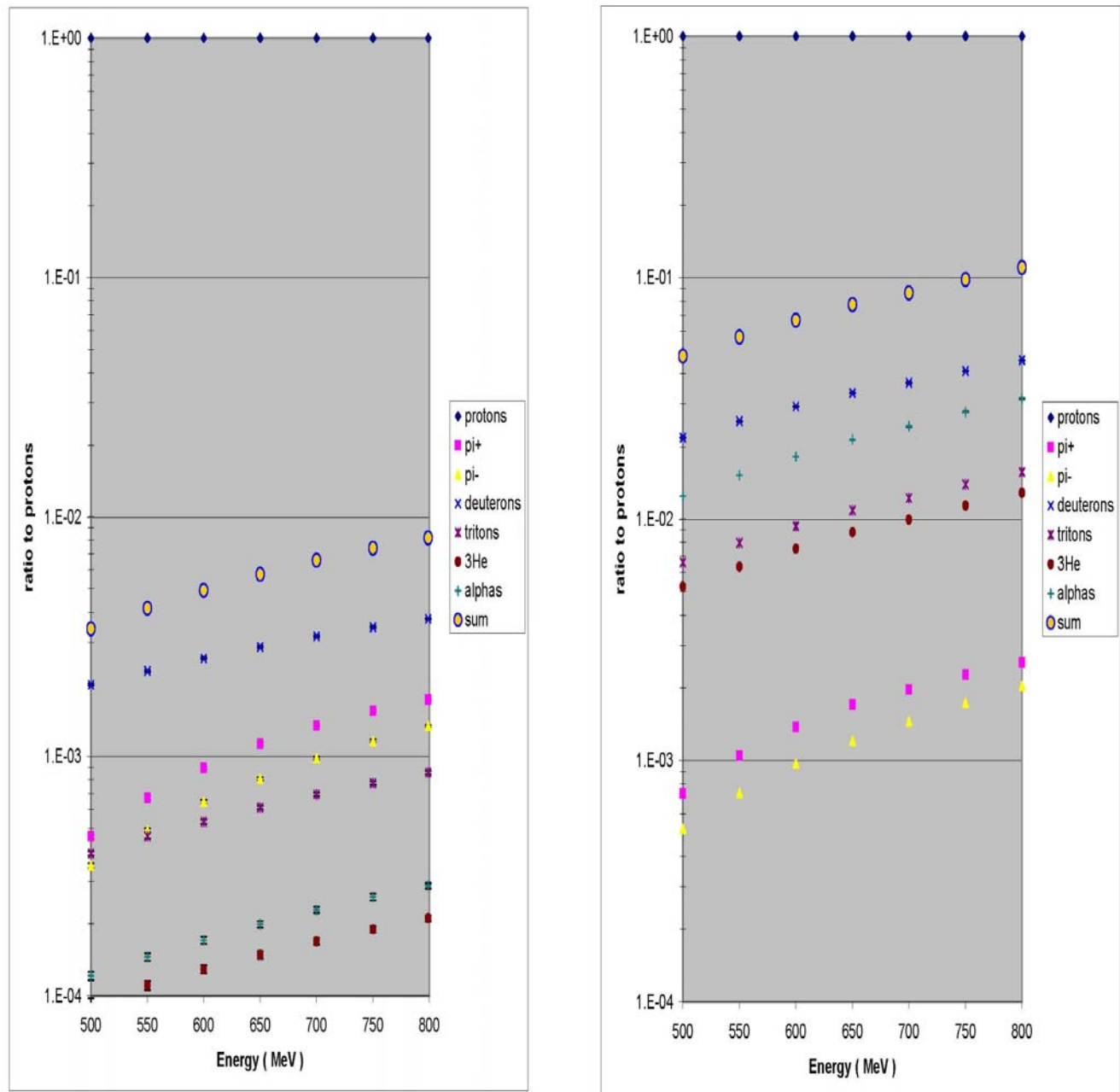


Figure 1a (left) – Ratio of the raw produced particle count (track length) to the proton count (track length) in an fmesh tally that overlays the LSO “detector”. This “detector” is one pixel that is 14-cm \times 14-cm \times 0.2-mm thick in beam direction located at 100 cm from the center of the window (Mode # 1). The particle type is indicated in the legend and sum is the sum of all particles excluding the protons. **Figure 1b** (right) is the same as 1a but the signal (track length) is multiplied by an energy dependent term. This term is the particles dE/dx as a function of energy divided by dE/dx for 1-GeV (1000-MeV) protons. The particle type is indicated in the legend and sum is the sum of all particles excluding the protons.

Energy (MeV)	Sum without multiplier		Sum with multiplier		Ratio of sum with to sum without	
		Error		Error		Error
800	0.00818	0.00004	0.11013	0.00014	13.46	0.07
750	0.00740	0.00004	0.09817	0.00015	13.27	0.07
700	0.00659	0.00004	0.08649	0.00012	13.12	0.07
650	0.00576	0.00003	0.07725	0.00011	13.42	0.08
600	0.00494	0.00003	0.06666	0.00010	13.49	0.09
550	0.00416	0.00003	0.05676	0.00010	13.66	0.10
500	0.00341	0.00003	0.04736	0.00009	13.88	0.11

Table III – The sum of the values in Table I (without multiplier) are compared to the sum in Table II (with multiplier), and the ratio of the two sums is given.

IV. The MCNP6 Model # 2

In preparing this document it was realized that the MCNP6 model with the LSO at 100 cm from the window center did not represent the real situation with the LSO as the detector. The problem was re-run for a more realistic case. In this case the LSO material starts 1-cm downstream of the center of the glass-Al window interface and is otherwise the same as Model #1. A MCNP geometry plot for this second case is shown in Figure 2.

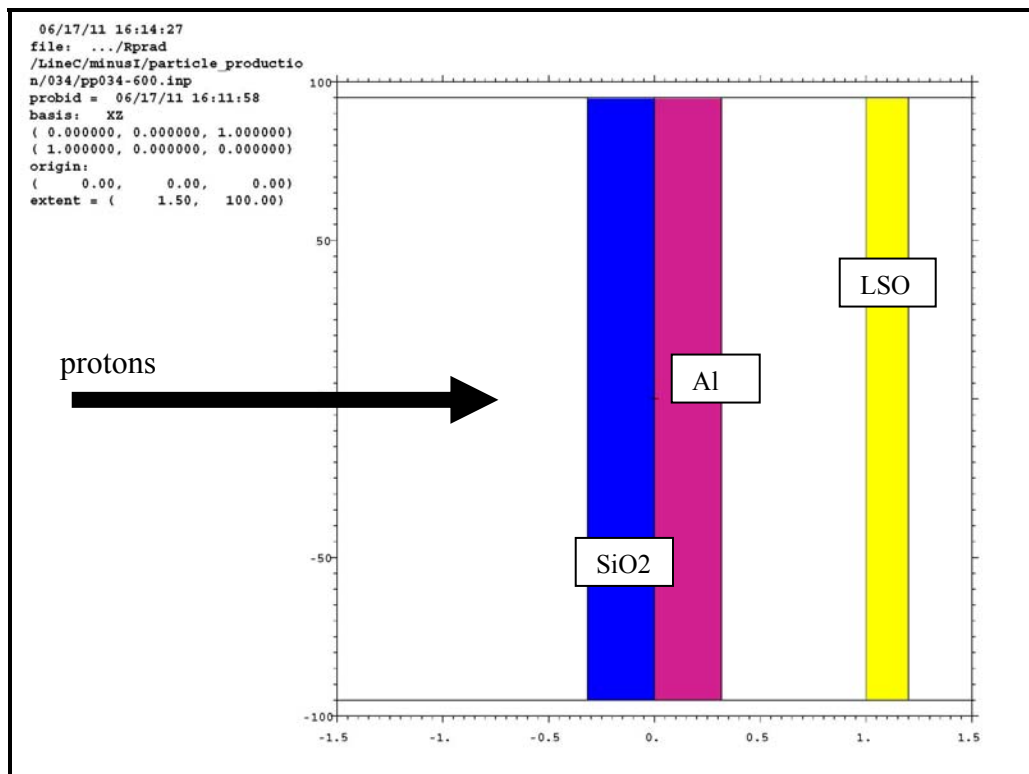


Figure 2 – MCNP geometry for the Model # 2 geometry (dimensions on the plot are in centimeters), note the aspect ratio of the plot is not 1-to-1. Protons are incident on the window (SiO₂ and Al) from the left (indicated by the arrow).

As in the case of Model # 1 results, various particles were tallied in fmesh (track length) tallies that were from -7 cm to +7 cm in both dimensions transverse to the z-axis and from 1.0 cm to 1.2 cm along the z-axis. There were separate fmesh tallies for protons, π^+ , π^- (charged pions), deuterons, tritons, helions (^3He) and alphas, with and without the energy dependent multiplier.

V. Results for Model #2

The results of the MCNP6 fmesh tallies are given in Table IV as a ratio to the proton fmesh tally for the Model # 2 (Figure 2) geometry. These results are also plotted in Figure 3a. Table V gives (plotted in Figure 3b) the results when an energy dependent multiplier (that is different for each particle) is applied. These multipliers were the same as the multipliers used for the Model # 1 results.

Energy (MeV)	π^+	Error	π^-	Error	d	Error	t	Error	^3He	Error	α	Error
800	4.51E-03	3.93E-06	2.37E-03	3.07E-06	6.32E-03	3.45E-06	1.07E-03	1.11E-06	2.82E-04	4.26E-07	2.95E-04	2.82E-07
750	4.01E-03	3.72E-06	2.03E-03	2.85E-06	5.88E-03	3.27E-06	9.63E-04	1.04E-06	2.54E-04	4.02E-07	2.64E-04	4.17E-07
700	3.48E-03	3.45E-06	1.69E-03	2.60E-06	5.43E-03	3.08E-06	8.66E-04	9.71E-07	2.28E-04	3.77E-07	2.33E-04	2.39E-07
650	2.90E-03	3.13E-06	1.37E-03	2.33E-06	4.95E-03	2.88E-06	7.64E-04	8.94E-07	2.01E-04	3.49E-07	2.03E-04	2.17E-07
600	2.30E-03	2.77E-06	1.08E-03	2.07E-06	4.44E-03	2.68E-06	6.67E-04	8.21E-07	1.75E-04	3.23E-07	1.74E-04	1.95E-07
550	1.72E-03	2.36E-06	8.02E-04	1.77E-06	3.93E-03	2.47E-06	5.78E-04	7.52E-07	1.49E-04	2.93E-07	1.48E-04	1.74E-07
500	1.19E-03	1.94E-06	5.58E-04	1.46E-06	3.41E-03	2.25E-06	4.89E-04	6.77E-07	1.24E-04	2.61E-07	1.23E-04	1.54E-07

Table IV – The values of the fmesh for the indicated particle as a ratio to the value for protons is given for the indicated proton energy.

Energy (MeV)	π^+	Error	π^-	Error	d	Error	t	Error	^3He	Error	α	Error
800	5.49E-03	5.20E-06	3.18E-03	4.18E-06	5.88E-02	3.03E-05	1.70E-02	1.47E-05	1.42E-02	1.67E-05	3.00E-02	2.24E-05
750	4.90E-03	4.92E-06	2.70E-03	3.85E-06	5.35E-02	2.82E-05	1.52E-02	1.36E-05	1.27E-02	1.55E-05	2.65E-02	3.25E-05
700	4.28E-03	4.57E-06	2.24E-03	3.48E-06	4.83E-02	2.61E-05	1.34E-02	1.26E-05	1.12E-02	1.43E-05	2.32E-02	1.86E-05
650	3.69E-03	4.28E-06	1.85E-03	3.19E-06	4.41E-02	2.46E-05	1.19E-02	1.19E-05	9.94E-03	1.34E-05	2.05E-02	1.71E-05
600	3.00E-03	3.84E-06	1.47E-03	2.82E-06	3.91E-02	2.25E-05	1.03E-02	1.03E-05	8.57E-03	1.23E-05	1.75E-02	1.5E-05
550	2.29E-03	3.31E-06	1.10E-03	2.42E-06	3.42E-02	2.05E-05	8.83E-03	9.67E-06	7.24E-03	1.11E-05	1.47E-02	1.3E-05
500	1.62E-03	2.74E-06	7.70E-04	2.00E-06	2.94E-02	1.84E-05	7.34E-03	8.57E-06	6.00E-03	9.83E-06	1.20E-02	1.17E-05

Table V – The values of the fmesh for the indicated particle as a ratio to the value for protons is given. This is for the case where each tally has an energy dependent multiplier that is dE/dx over dE/dx of a 1-GeV proton. Note that these tally multipliers are different for each particle type.

One sees in general that the values in Tables IV and V (Model # 2) are greater than the values in Tables I and II (Model # 1) but the ratios of the sum with multiplier to sum without multiplier for Model # 2 (Table VI) are less than the values for Model # 1 (Table III). There are at least two effects: one is the fact that the solid angle for particles off the window getting to the LSO will be greater for Model # 2 than for Model # 1. A second effect is that the energy spectrum of the particles getting to the LSO in the two cases could be and probably is different.

While we have not tabulated the results here, there is a number of charged muons getting to the LSO in the Model # 2 case (these were not recorded in the Model #1 case) – these muons presumably coming from charged-pion decay and are 5% to 8% of the π^+ /p ratios and ~0.2% of the π^- /p ratios.

Energy (MeV)	Sum without multiplier		Sum with multiplier		Ratio of sum with to sum without	
		Error		Error		Error
800	0.01485	0.00001	0.12868	0.00004	8.67	< 0.01
750	0.01340	0.00001	0.11550	0.00005	8.62	0.01
700	0.01193	0.00001	0.10252	0.00004	8.59	0.01
650	0.01038	< 0.00001	0.09203	0.00004	8.87	0.01
600	0.00884	< 0.00001	0.07989	0.00003	9.04	0.01
550	0.00732	< 0.00001	0.06831	0.00003	9.33	0.01
500	0.00589	< 0.00001	0.05714	0.00003	9.70	0.01

Table VI – The sum of the values in Table IV (without multiplier) are compared to the sum in Table V (with multiplier), and the ratio of the two sums is given. This is for the MCNP geometry Model # 2 case.

For Model # 2 we have also calculation the image of the particles in the LSO with a mesh that is 1400 pixels -by- 1400 pixels -by- 1 pixel thick covering 14-cm \times 14-cm \times 0.2-cm. These images divided by the summed image (protons + π^+ + π^- + μ^+ + μ^- + deuterons + tritons + 3He + α) are shown in Figure 4a-i, respectively, on plots that cover two orders of magnitude in the intensity scale; and in Figure 5a-i where the lower bound of the intensity is auto scaled for each plot.

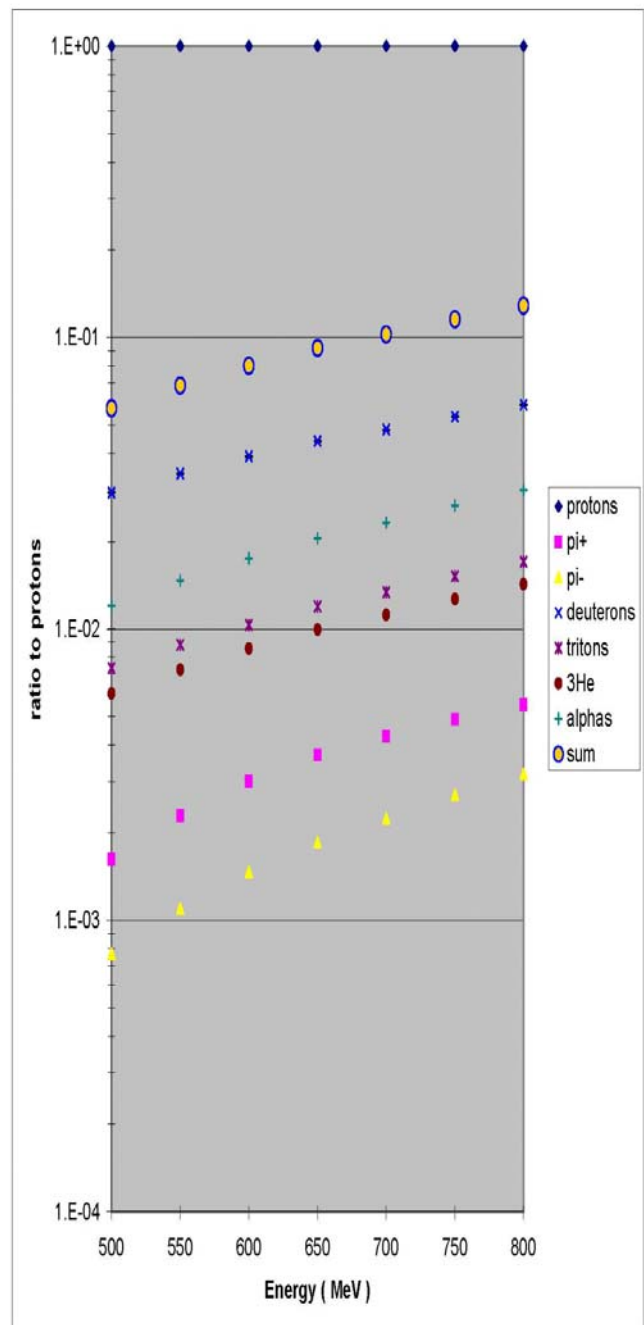
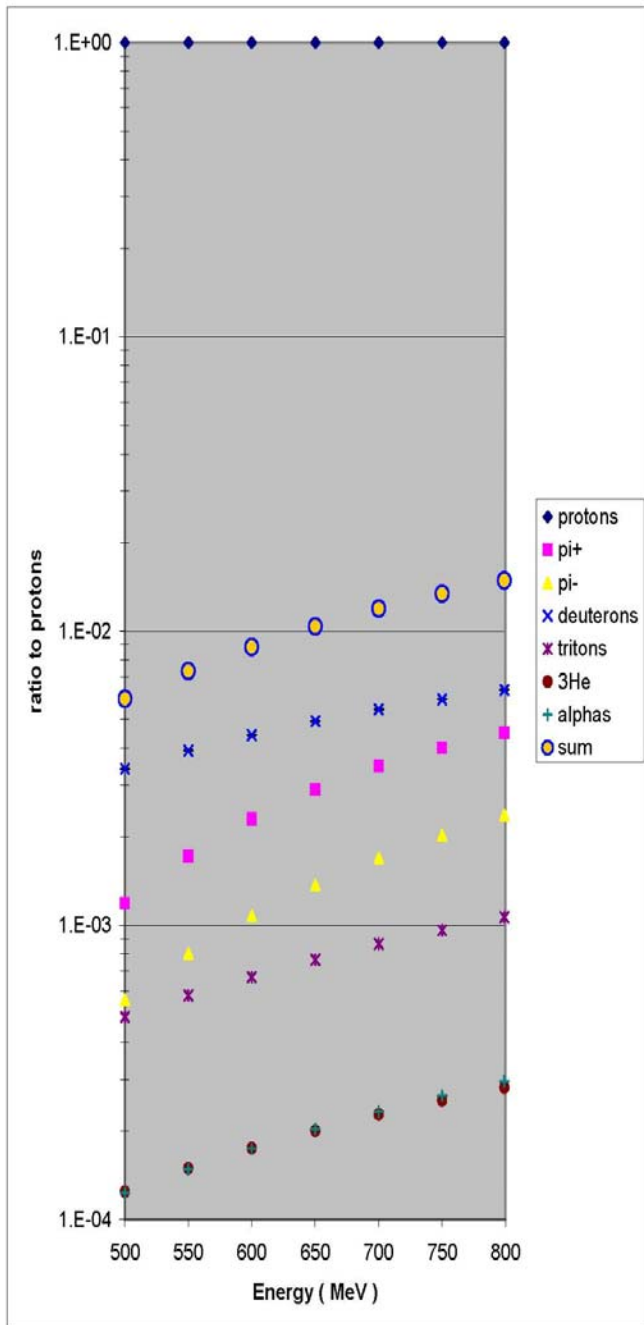


Figure 3a and 3b (left) – Caption is the same as Figure 1a and 1b except that runs were with MCNP Model #2 (see text) with LSO detector 1 cm from the center of the window.

Protons from 800-MeV protons with SiO₂-Al window and LSO

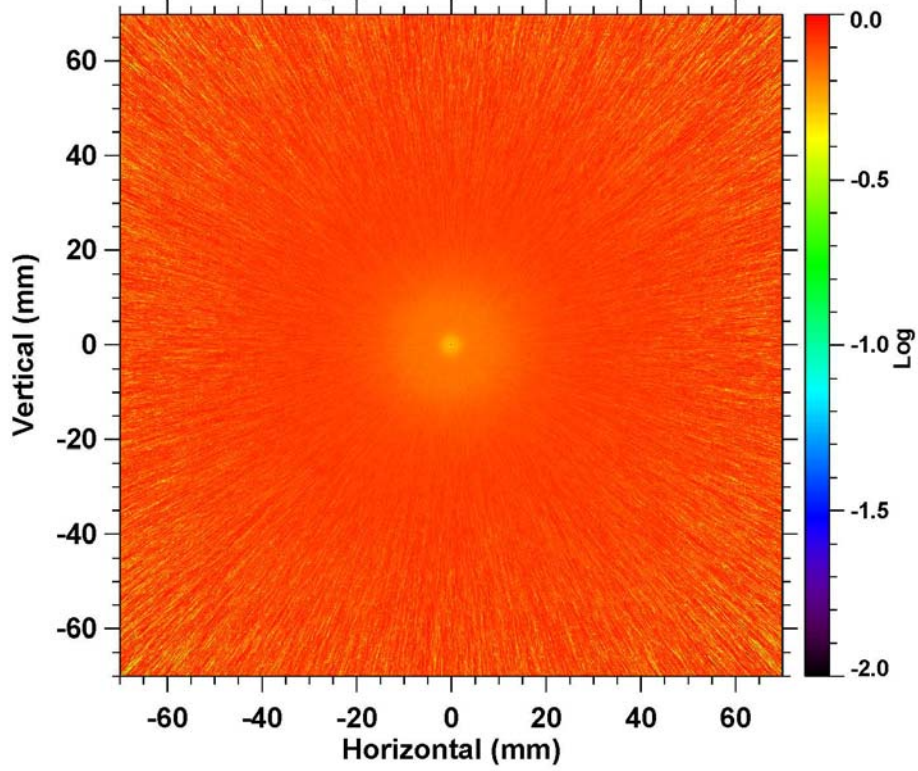
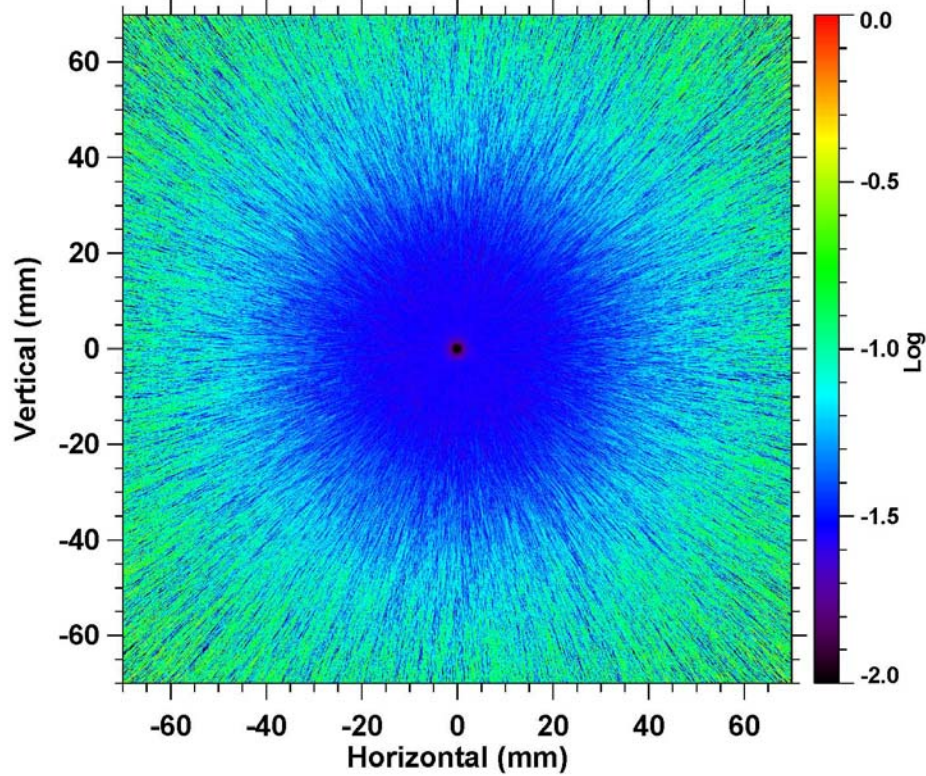
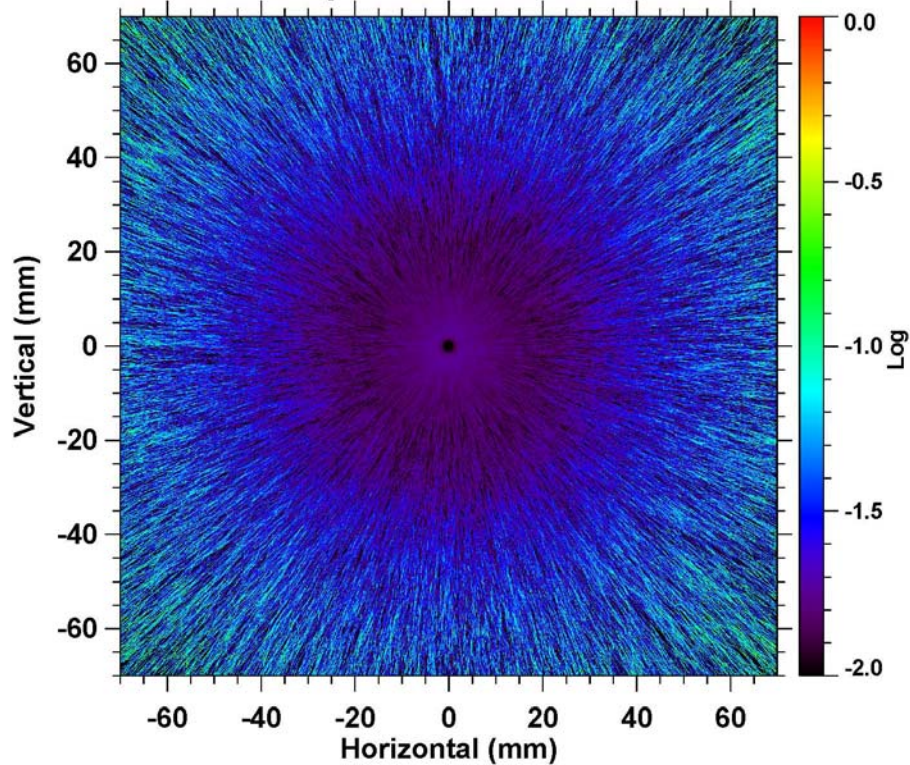


Figure 4a – Ratio of the proton image to the summed image (see text).

Pi-plus from 800-MeV protons with SiO2-Al window and LSOFigure 4b – Ratio of the π^+ image to the summed image (see text).**Pi-minus from 800-MeV protons with SiO2-Al window and LSO**Figure 4c – Ratio of the π^- image to the summed image (see text).

Mu-plus from 800-MeV protons with SiO₂-Al window and LSO

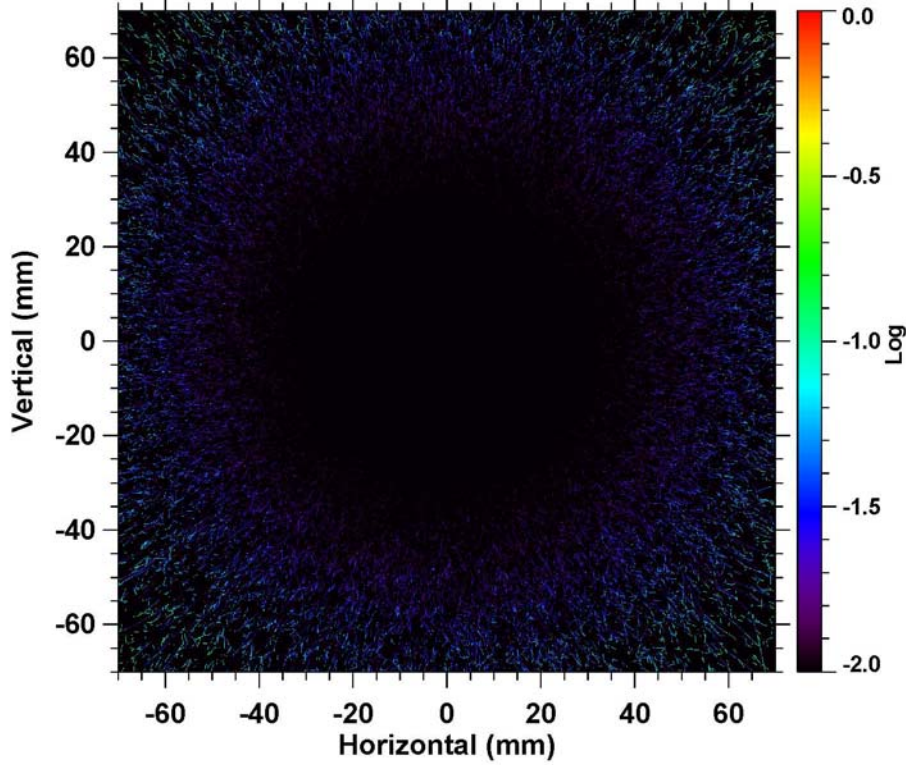


Figure 4d – Ratio of the μ^+ image to the summed image (see text).

Mu-minus from 800-MeV protons with SiO₂-Al window and LSO

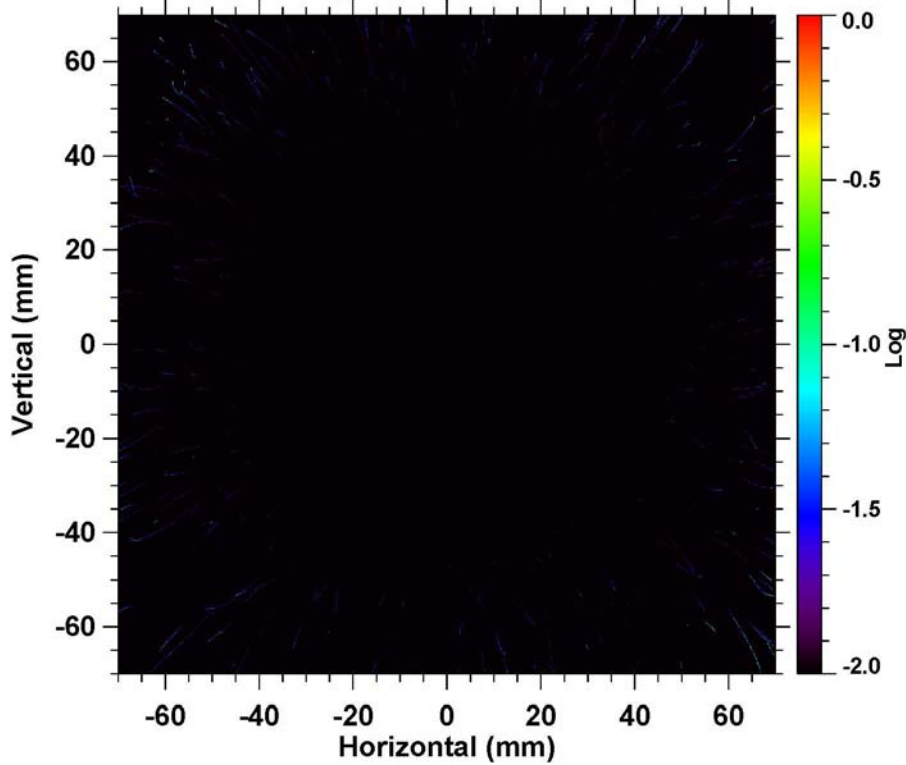


Figure 4e – Ratio of the μ^- image to the summed image (see text).

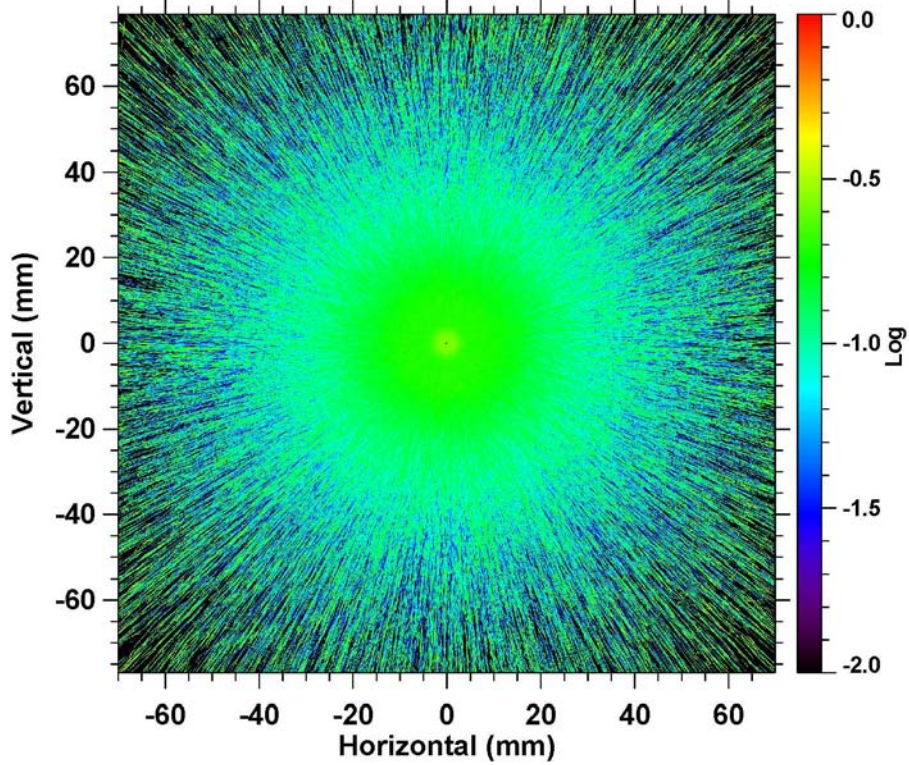
Deuterons from 800-MeV protons with SiO₂-Al window and LSO

Figure 4f – Ratio of the deuteron image to the summed image (see text).

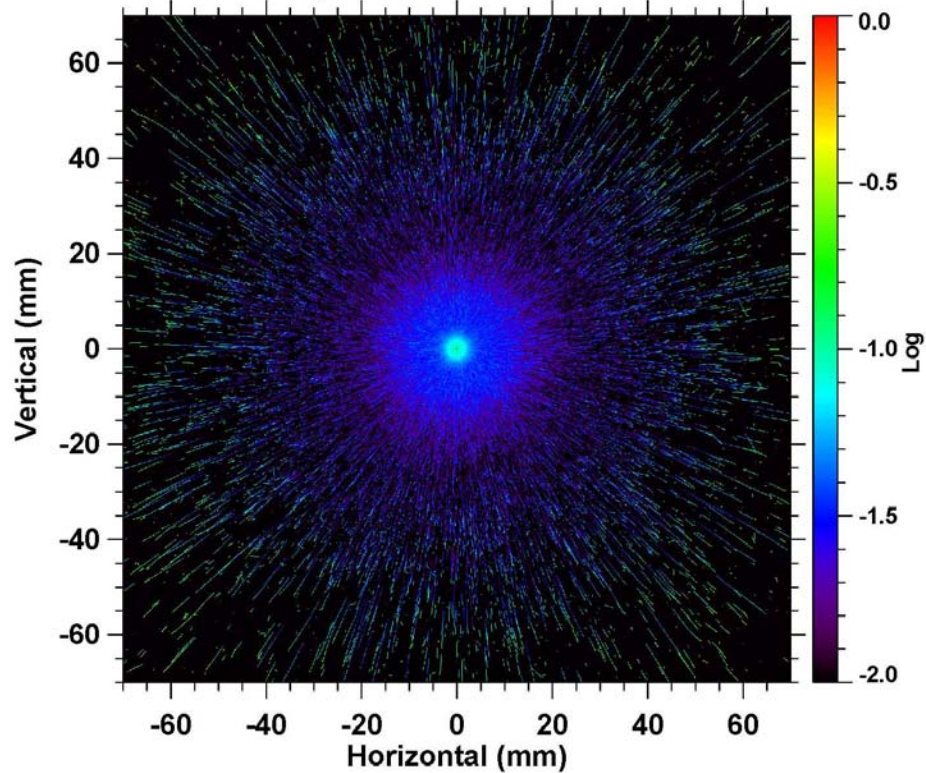
Tritons from 800-MeV protons with SiO₂-Al window and LSO

Figure 4g – Ratio of the triton image to the summed image (see text).

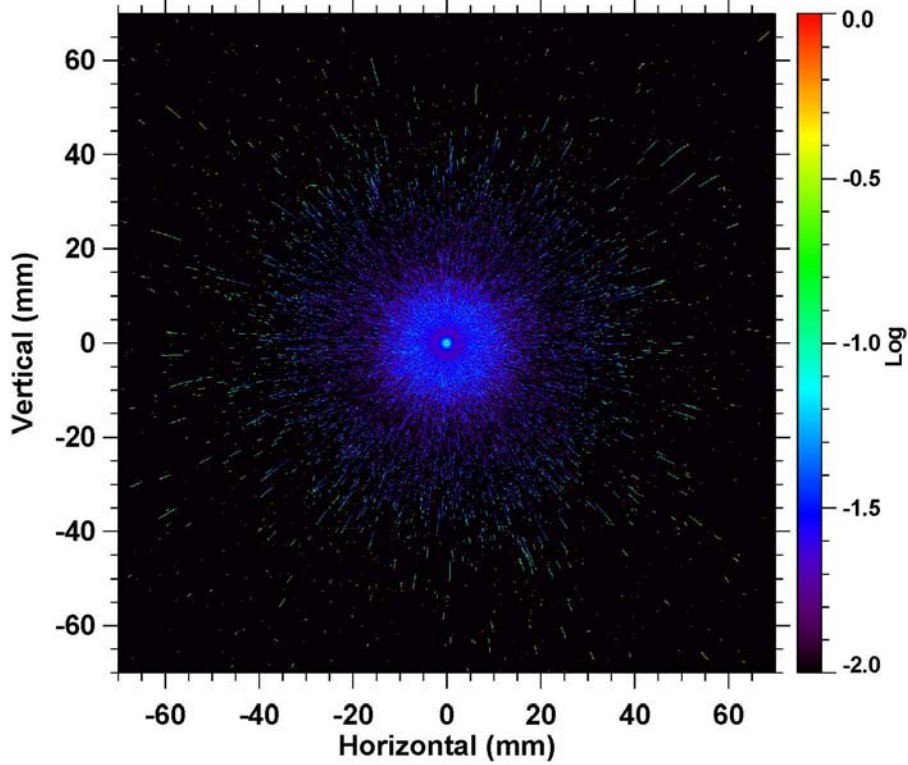
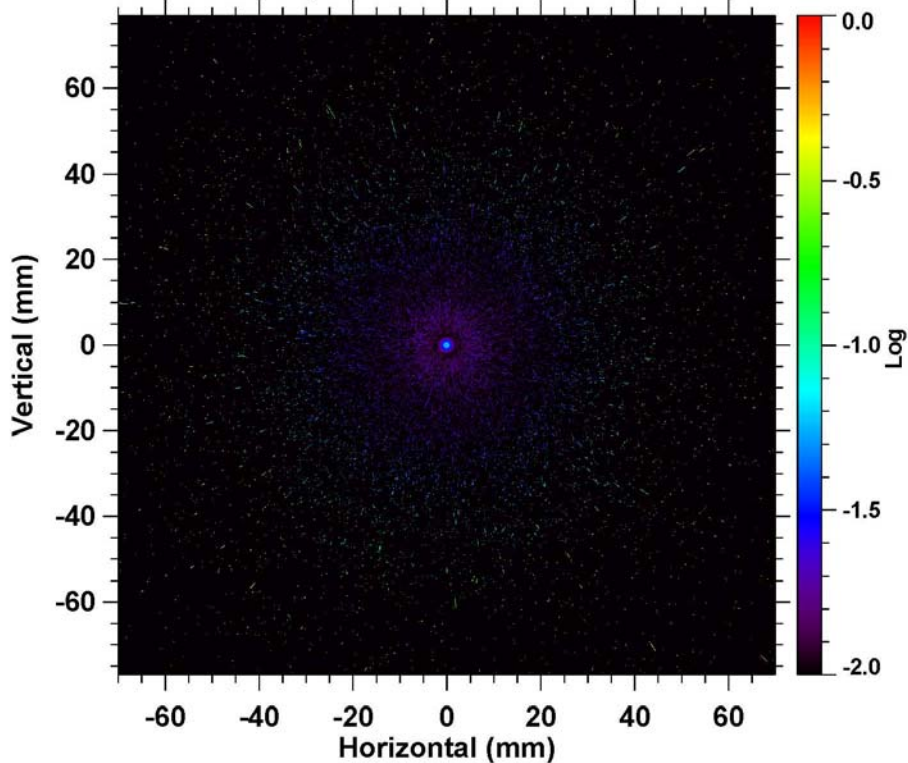
^3He from 800-MeV protons with SiO₂-Al window and LSOFigure 4h – Ratio of the ^3He image to the summed image (see text).**Alphas from 800-MeV protons with SiO₂-Al window and LSO**

Figure 4i – Ratio of the alpha particle image to the summed image (see text).

Protons from 800-MeV protons with SiO₂-Al window and LSO

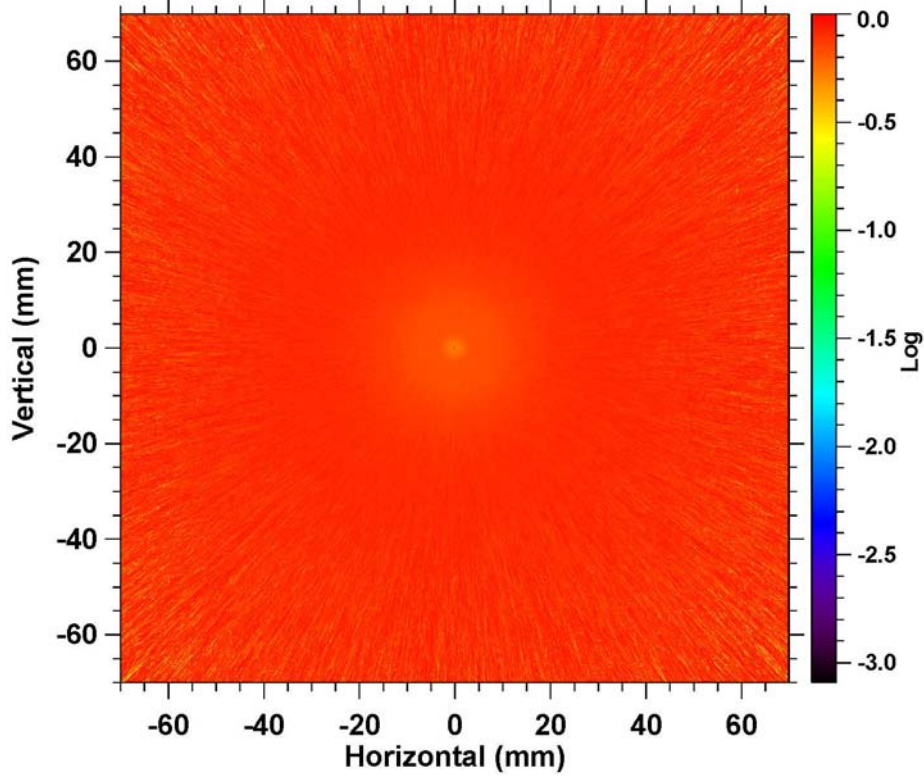


Figure 5a – Ratio of the proton image to the summed image with the lower limit of the intensity scale auto scaled by the plotting program. This is the same data as in Figure 4a.

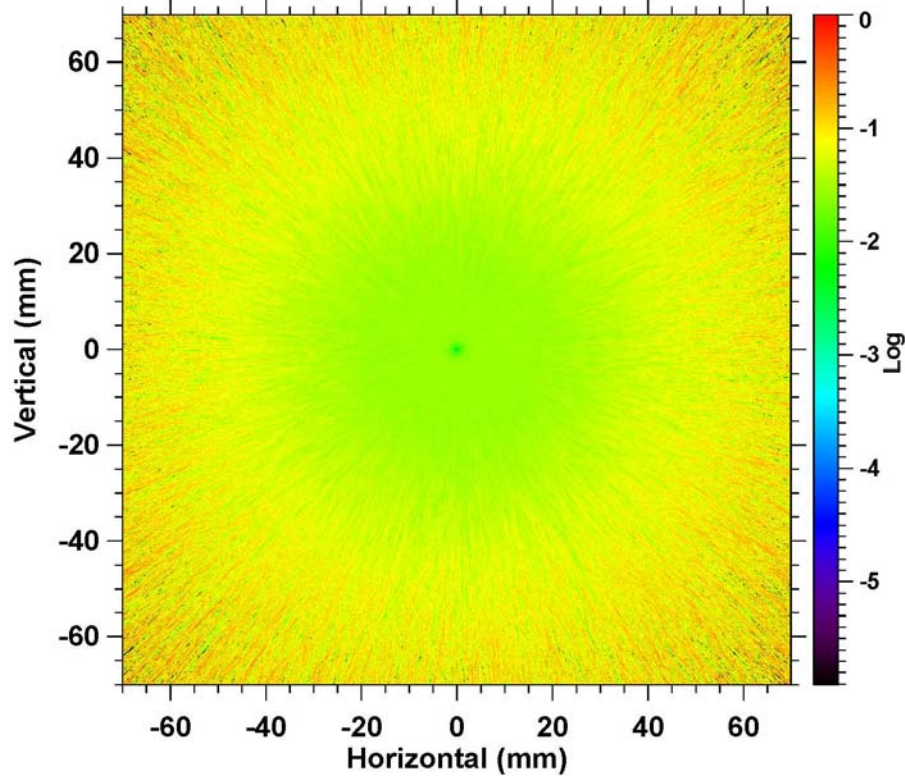
Pi-plus from 800-MeV protons with SiO₂-Al window and LSO

Figure 5b – Ratio of the π^+ image to the summed image with the lower limit of the intensity scale auto scaled by the plotting program. This is the same data as in Figure 4b.

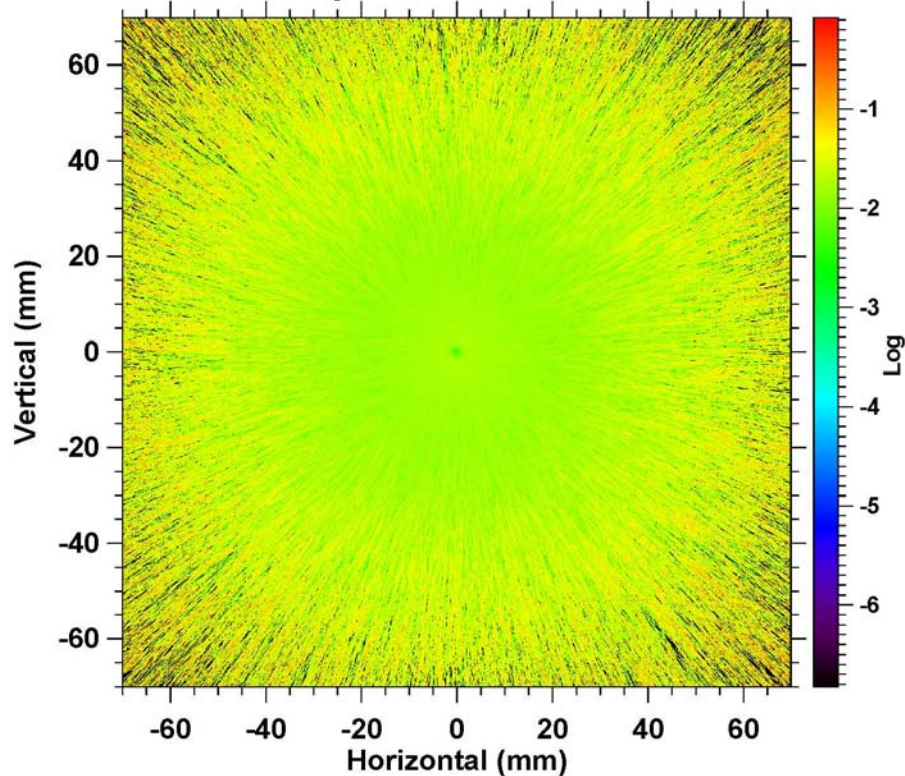
Pi-minus from 800-MeV protons with SiO₂-Al window and LSO

Figure 5c – Ratio of the π^- image to the summed image with the lower limit of the intensity scale auto scaled by the plotting program. This is the same data as in Figure 4c.

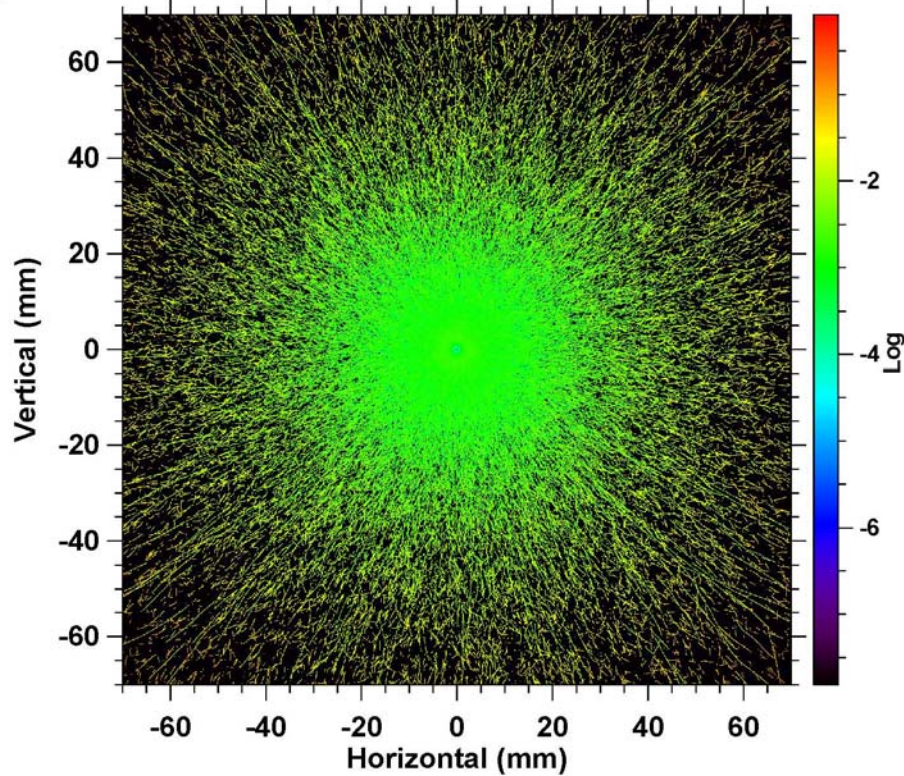
Mu-plus from 800-MeV protons with SiO₂-Al window and LSO

Figure 5d – Ratio of the proton image to the summed image with the lower limit of the intensity scale auto scaled by the plotting program. This is the same data as in Figure 4d.

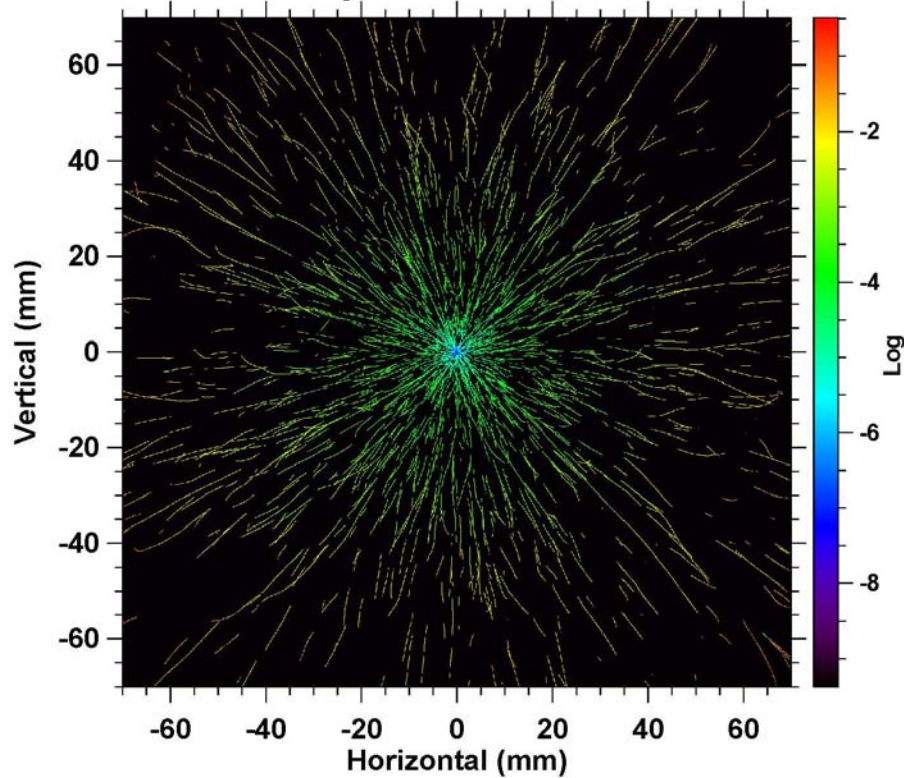
Mu-minus from 800-MeV protons with SiO₂-Al window and LSO

Figure 5e – Ratio of the proton image to the summed image with the lower limit of the intensity scale auto scaled by the plotting program. This is the same data as in Figure 4e.

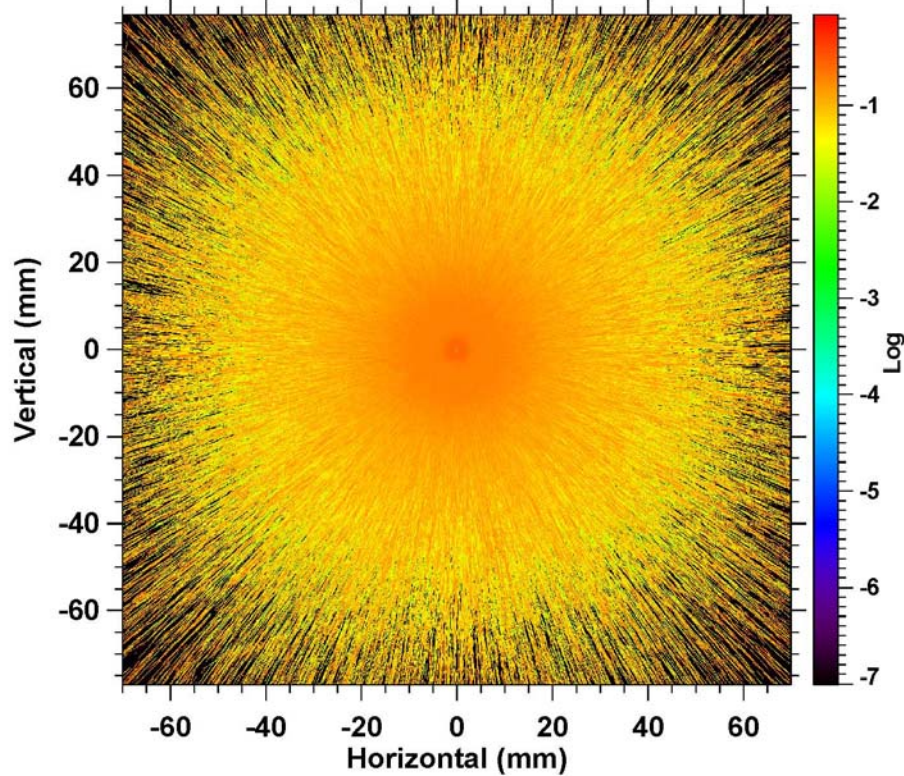
Deuterons from 800-MeV protons with SiO₂-Al window and LSO

Figure 5f – Ratio of the proton image to the summed image with the lower limit of the intensity scale auto scaled by the plotting program. This is the same data is in Figure 4f.

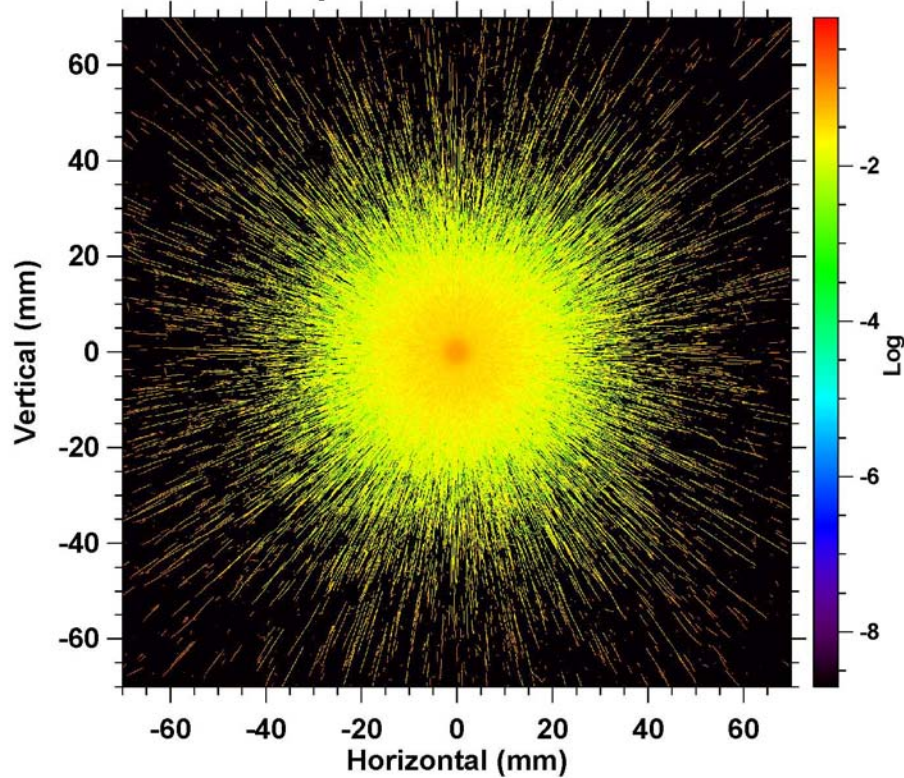
Tritons from 800-MeV protons with SiO₂-Al window and LSO

Figure 5g – Ratio of the proton image to the summed image with the lower limit of the intensity scale auto scaled by the plotting program. This is the same data is in Figure 4g.

^3He from 800-MeV protons with $\text{SiO}_2\text{-Al}$ window and LSO

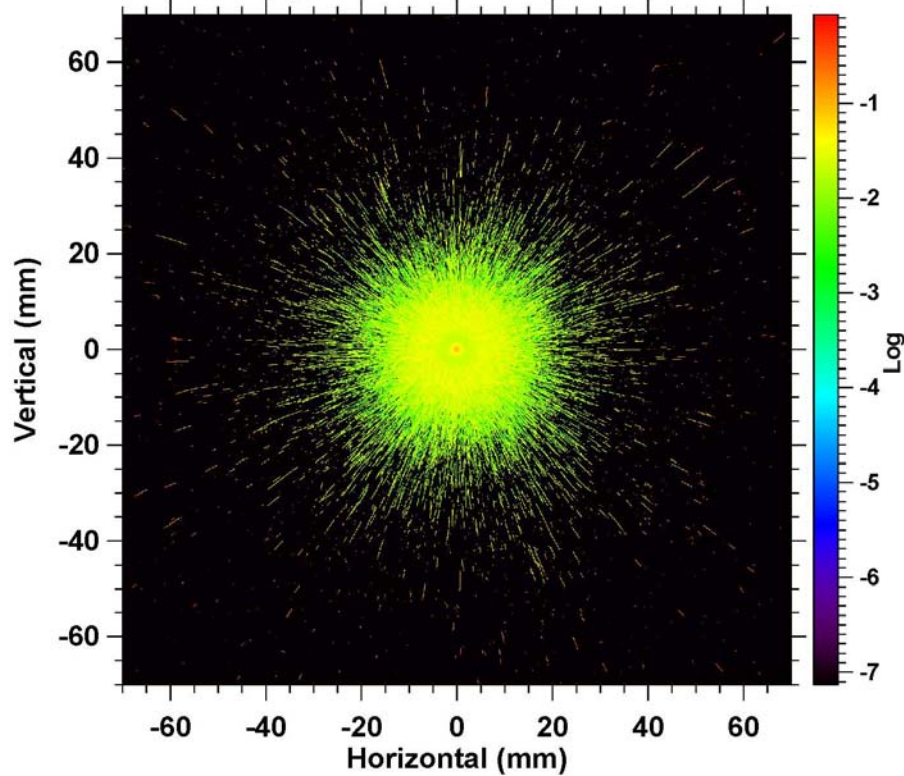


Figure 5h – Ratio of the proton image to the summed image with the lower limit of the intensity scale auto scaled by the plotting program. This is the same data as in Figure 4h.

Alphas from 800-MeV protons with $\text{SiO}_2\text{-Al}$ window and LSO

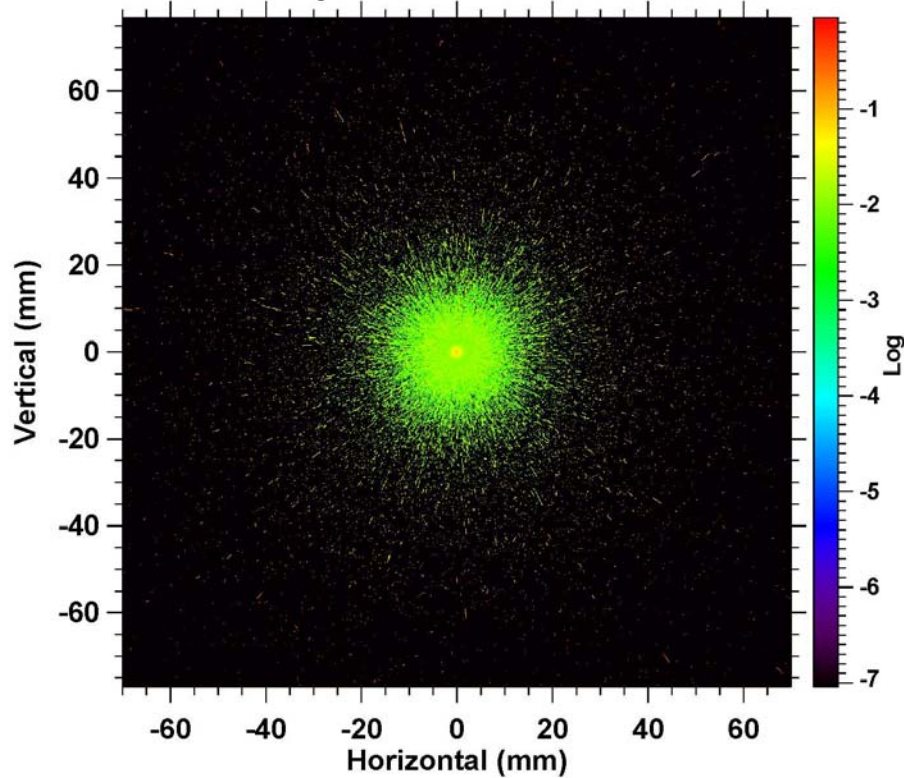


Figure 5i – Ratio of the proton image to the summed image with the lower limit of the intensity scale auto scaled by the plotting program. This is the same data as in Figure 4i.

VI. Conclusions

Monte Carlo calculations with MCNP6 of a protons incident of a thick window (similar to the window used in some proton radiography experiments at Line C) and subsequently transported to a LSO detector show a significant number of secondary particles in the LSO. If a model that accounts for the relative energy loss of the particles in the LSO is applied one sees that the summed signal from the secondary particles is 5% to 12% of the proton signal depending on the incident proton energy.

The effects of these secondary particles should cancel out when the experimenters calculate a transmission by taking the ratio of an object-in run to an object-out run. However, one must be careful since there appears to be energy dependence to the secondary contribution, and the protons energies for the object-in run and the object-out run will probably be different.

The secondary production in the window and subsequent spreading of signal in the LSO scintillator (Figures 4b through 4i) might lead to the effect that has been called “long range blur”. The effect of long range blur has been discussed in a couple of documents.³ These documents discuss the effect at LANSCE Line C (800-MeV protons) and at the Brookhaven AGS (24-GeV/c protons), respectively, and the latter points out that the long range blur is reduced by approximately an order of magnitude at the energy higher energy. If it is secondary particle production causing the effect then the forward peaking at energy proton energies might explain the effect. We intend to perform similar MCNP6 calculations at the higher energy when the cross sections become available in the code – the cross sections currently stop at ~5-GeV proton energy.

It should be noted that the calculations presented in this note do not include delta rays (i.e. fast electrons produced by the energetic charged particles knocking orbiting electrons out of atoms), or heavy ions (i.e. ions heavier than alpha particles that could be produced primarily by the protons interacting with the nuclei of the window material(s)). Both of these processes would modify the scintillator signal, but neither process is included in MCNP6 at the moment.

VII. References

1. “Initial MCNP6 Release Overview”, T. Goorley et al., LA-UR-11-01766 -- states: “While MCNP6 is simply and accurately described as the merger of MCNP5 and MCNPX capabilities, it is also the result of 4 years of meticulous effort by the MCNP5 and MCNPX code development teams.”

The merger is cited is being or nearing completion, but this author will believe this when it is seen at RSICC (Radiation Safety Information Computational Center).

2. “CEM03.03 and LAQGSM03.03 Event Generators for the MCNP6, MCNPX, and MARS15 Transport Codes”, S. G. Mashnik, K. K. Gudima, R. E. Prael, A. J. Sierk, M. I. Baznat, and N. V. Mokhov, Joint ICTP-IAEA Advanced Workshop on Model Codes for Spallation Reactions, February 4-8, 2008, ICTP, Trieste, Italy; LA-UR-08-2931; E-print: arXiv:0805.0751v2 [nucl-th]; IAEA Report INDC(NDS)-0530, Distr. SC, Vienna, Austria, August 2008, p. 51.

3. “Long Range Blur correction to Proton Radiography Data”, N. S. P. King, K. B. Morley, C. L. Morris and Pete Pazuchanics, Los Alamos National Laboratory (no date and no LA number); “Tile Glow Correction” Chris Morris et al., LANL, LLNL, and Bechtel Nevada (no date and no LA number).

VIII. Acknowledgements

Thanks to my fellow transporters in XCP-7 “Transport Applications” for the occasional discussion of this and similar topics. And also to XCP-3 “Monte Carlo Codes” for the implementation of the new features that allow proton radiography simulations with MCNP6, and in advance for features that are yet to be implemented.

JDZ:jdz

Appendix I — MCNP6 input for Model # 2 geometry

```

file: .../Rprad/LineC/minusI/particle_production/035/pp035-700.inp
c from .../Rprad/LineC/minusI/particle_production/034/pp034-700.inp
c from .../Rprad/LineC/minusI/particle_production/018/pp018.inp
c
c to 1400x1400-pixel LSO detector that is 14-cm by 14-cm by 0.2-cm thick
c location 1-cm to 1.2-cm downstream of center of window
c
c particle production with 700-MeV protons
c with 'tropt' card
c and proton cutoff set to 10-MeV
c DF cards are dE/dX(E) to proton stopping power at 1-GeV
c
c start cell cards
c
101  0          -50  101  -102      imp:h=1
102  14  -2.65   -50  102  -103      imp:h=1
103  13  -2.70   -50  103  -104      imp:h=1
104  0          -50  104  -105      imp:h=1
105  71  -7.36   -50  105  -106      imp:h=1
106  0          -50  106  -107      imp:h=1
c
75  0          50:-101:+107      imp:h=0
c -----
c end of cell cards

c start surface cards
50  cz  95
c
101  pz  -100
102  pz  -0.3175
103  pz  0.0000
104  pz  0.3175
105  pz  1
106  pz  1.2
107  pz  100
c -----
c end of surface cards

c start physics cards
c mode h
mode h / * | ! d t s a
c phys:n 1000
phys:h 1000
phys:/ 1000
phys:* 1000
phys:| 1000
phys:! 1000
phys:d 1000
phys:t 1000
phys:s 1000
phys:a 1000
c
c cut:n j 1.00
cut:h j 5.
cut:/ j 5.
cut:* j 5.
cut:| j 5.
cut:! j 5.
cut:d j 5.
cut:t j 5.
cut:s j 5.
cut:a j 5.
c
tropt nreact=on nescat=on mcscat=fnal1 eloss=strag1
c void
c -----

```

```

sdef erg=700. part=5 sur=101 x=0 y=0 z=-100 vec=0 0 1 dir=1
C -----
rand gen=2
print -160 -30
C -----
nps          1000000000
prtmp j      100000000 1 2 100000000
C -----
m13 13027 1.          $ aluminum
m14 14028 1. 08016 2. $ SiO2 == glass (rho=2.64 g/cc)
m71 71175 2. 14028 1. 8016 5. $ LSO (rho=7.36 g/cc)
c end of material cards
C -----
fc021 exit of problem
f021:h 105
e021 0 001 800i 802
C -----
fc031 exit of problem
f031:n 105
e031 0 001 800i 802
C -----
fc411 pi+ at exit of problem
f411:/ 105
e411 00 99i 1000
C -----
fc511 pi- just after object energy
f511:* 105
e511 00 99i 1000
C -----
fc611 mu+ just after object energy
f611:! 105
e611 00 99i 1000
C -----
fc711 mu- just after object energy
f711:| 105
e711 00 99i 1000
C -----
fc811 deuterons just after object energy
f811:d 105
e811 00 99i 1000
C -----
fc911 tritons just after object energy
f911:t 105
e911 00 99i 1000
C -----
fc1011 3He just after object energy
f1011:s 105
e1011 00 99i 1000
C -----
fc1111 alphas just after object energy
f1111:a 105
e1111 00 99i 1000
C -----
C -----
C -----
C -----
fc154 proton image at IL1
fmesh154:h geom=rec origin=-7 -7 +1.0
imesh 7 iints 1400
jmesh 7 jints 1400 kmesh +1.2 out=cf
DE154 LIN 5.06578 5.52427 6.02426 6.56950 7.16409 7.81250
          8.51959 9.29068 10.13160 11.04850 12.04850 13.13900
          14.32820 15.62500 17.03920 18.58140 20.26310 22.09710
          24.09700 26.27800 28.65640 31.25000 34.07840 37.16270
          40.52620 44.19420 48.19410 52.55600 57.31280 62.50000
          68.15670 74.32540 81.05250 88.38830 96.38820 105.11200
          114.62600 125.00000 136.31300 148.65100 162.10500 176.77699
          192.77600 210.22400 229.25101 250.00000 272.62701 297.30200
          324.20999 353.55301 385.55301 420.44800 458.50201 500.00000

```

	545.25403	594.60400	648.41998	707.10699	771.10498	840.89600
	917.00403	1000.00000				
DF154 LIN	26.08269	24.42458	23.06607	23.06607	20.53502	19.36003
	18.24370	17.18285	16.17851	16.17851	14.32689	13.47228
	12.66411	11.90028	11.17743	11.17743	9.85530	9.24868
	8.67966	8.14292	7.63895	7.63895	6.72014	6.30293
	5.91134	5.54462	5.20113	5.20113	4.57863	4.29743
	4.03476	3.78938	3.56046	3.56046	3.14812	2.96289
	2.79043	2.63060	2.48150	2.48150	2.21463	2.09555
	1.98528	1.88349	1.78915	1.78915	1.62186	1.54794
	1.48000	1.41767	1.36058	1.36058	1.26090	1.21772
	1.17860	1.14331	1.11163	1.11163	1.05821	1.03608
	1.01673	1.00000				

C -----

```
fc454 pi+ image at IL1
fmesh454:/ geom=rec origin=-7 -7 +1.0
imesh 7 iints 1400
jmesh 7 jints 1400 kmesh +1.2 out=cf
```

DE454 LIN	5.06578	5.52427	6.02426	6.56950	7.16409	7.81250
	8.51959	9.29068	10.13160	11.04850	12.04850	13.13900
	14.32820	15.62500	17.03920	18.58140	20.26310	22.09710
	24.09700	26.27800	28.65640	31.25000	34.07840	37.16270
	40.52620	44.19420	48.19410	52.55600	57.31280	62.50000
	68.15670	74.32540	81.05250	88.38830	96.38820	105.11200
	114.62600	125.00000	136.31300	148.65100	162.10500	176.77699
	192.77600	210.22400	229.25101	250.00000	272.62701	297.30200
	324.20999	353.55301	385.55301	420.44800	458.50201	500.00000
	545.25403	594.60400	648.41998	707.10699	771.10498	840.89600
	917.00403	1000.00000				

DF454 LIN	6.71911	6.30202	5.91054	5.91054	5.20051	4.87881	\$ ratio of pion dE/dx values
	4.57813	4.29698	4.03435	4.03435	3.56011	3.34675	\$ to proton dE/dx at 1-GeV
	3.14781	2.96259	2.79015	2.79015	2.48122	2.34276	
	2.21435	2.09526	1.98498	1.98498	1.78884	1.70182	
	1.62152	1.54759	1.47963	1.47963	1.36017	1.30801	
	1.26047	1.21727	1.17812	1.17812	1.11110	1.08277	
	1.05764	1.03548	1.01609	1.01609	0.98504	0.97297	
	0.96294	0.95483	0.94849	0.94849	0.94066	0.93894	
	0.93854	0.93936	0.94129	0.94129	0.94811	0.95282	
	0.95829	0.96445	0.97121	0.97121	0.98629	0.99448	
	1.00303	1.01189					

C -----

```
fc554 pi- image at IL1
fmesh554:* geom=rec origin=-7 -7 +1.0
imesh 7 iints 1400
jmesh 7 jints 1400 kmesh +1.2 out=cf
```

DE554 LIN	5.06578	5.52427	6.02426	6.56950	7.16409	7.81250
	8.51959	9.29068	10.13160	11.04850	12.04850	13.13900
	14.32820	15.62500	17.03920	18.58140	20.26310	22.09710
	24.09700	26.27800	28.65640	31.25000	34.07840	37.16270
	40.52620	44.19420	48.19410	52.55600	57.31280	62.50000
	68.15670	74.32540	81.05250	88.38830	96.38820	105.11200
	114.62600	125.00000	136.31300	148.65100	162.10500	176.77699
	192.77600	210.22400	229.25101	250.00000	272.62701	297.30200
	324.20999	353.55301	385.55301	420.44800	458.50201	500.00000
	545.25403	594.60400	648.41998	707.10699	771.10498	840.89600
	917.00403	1000.00000				

DF554 LIN	6.71911	6.30202	5.91054	5.91054	5.20051	4.87881	\$ ratio of pion dE/dx values
	4.57813	4.29698	4.03435	4.03435	3.56011	3.34675	\$ to proton dE/dx at 1-GeV
	3.14781	2.96259	2.79015	2.79015	2.48122	2.34276	
	2.21435	2.09526	1.98498	1.98498	1.78884	1.70182	
	1.62152	1.54759	1.47963	1.47963	1.36017	1.30801	
	1.26047	1.21727	1.17812	1.17812	1.11110	1.08277	
	1.05764	1.03548	1.01609	1.01609	0.98504	0.97297	
	0.96294	0.95483	0.94849	0.94849	0.94066	0.93894	
	0.93854	0.93936	0.94129	0.94129	0.94811	0.95282	
	0.95829	0.96445	0.97121	0.97121	0.98629	0.99448	
	1.00303	1.01189					

C -----

```
fc654 mu+ image at IL1
fmesh654:! geom=rec origin=-7 -7 +1.0
```

```

imesh 7 iints 1400
jmesh 7 jints 1400      kmesh  +1.2  out=cf
DE654 LIN  5.06578  5.52427  6.02426  6.56950  7.16409  7.81250
            8.51959  9.29068  10.13160  11.04850  12.04850  13.13900
            14.32820  15.62500  17.03920  18.58140  20.26310  22.09710
            24.09700  26.27800  28.65640  31.25000  34.07840  37.16270
            40.52620  44.19420  48.19410  52.55600  57.31280  62.50000
            68.15670  74.32540  81.05250  88.38830  96.38820  105.11200
            114.62600  125.00000  136.31300  148.65100  162.10500  176.77699
            192.77600  210.22400  229.25101  250.00000  272.62701  297.30200
            324.20999  353.55301  385.55301  420.44800  458.50201  500.00000
            545.25403  594.60400  648.41998  707.10699  771.10498  840.89600
            917.00403  1000.00000
DF654 LIN  5.46768  5.12906  4.81208  4.81208  4.23864  3.97987 $ ratio of muon dE/dx values
            3.73813  3.51271  3.30252  3.30252  2.92424  2.75446 $ to proton dE/dx at 1-GeV
            2.59712  2.45038  2.31414  2.31414  2.07065  1.96219
            1.86209  1.76934  1.68382  1.68382  1.53230  1.46558
            1.40439  1.34837  1.29722  1.29722  1.20832  1.17001
            1.13548  1.10451  1.07689  1.07689  1.03084  1.01203
            0.99580  0.98199  0.97036  0.97036  0.95301  0.94702
            0.94266  0.93981  0.93837  0.93837  0.93926  0.94139
            0.94451  0.94855  0.95341  0.95341  0.96525  0.97210
            0.97946  0.98728  0.99551  0.99551  1.01294  1.02205
            1.03136  1.04084

```

C -----

```

fc754 mu-      image at IL1
fmesh754:| geom=rec origin=-7 -7 +1.0
imesh 7 iints 1400
jmesh 7 jints 1400      kmesh  +1.2  out=cf
DE754 LIN  5.06578  5.52427  6.02426  6.56950  7.16409  7.81250
            8.51959  9.29068  10.13160  11.04850  12.04850  13.13900
            14.32820  15.62500  17.03920  18.58140  20.26310  22.09710
            24.09700  26.27800  28.65640  31.25000  34.07840  37.16270
            40.52620  44.19420  48.19410  52.55600  57.31280  62.50000
            68.15670  74.32540  81.05250  88.38830  96.38820  105.11200
            114.62600  125.00000  136.31300  148.65100  162.10500  176.77699
            192.77600  210.22400  229.25101  250.00000  272.62701  297.30200
            324.20999  353.55301  385.55301  420.44800  458.50201  500.00000
            545.25403  594.60400  648.41998  707.10699  771.10498  840.89600
            917.00403  1000.00000
DF754 LIN  5.46768  5.12906  4.81208  4.81208  4.23864  3.97987 $ ratio of muon dE/dx values
            3.73813  3.51271  3.30252  3.30252  2.92424  2.75446 $ to proton dE/dx at 1-GeV
            2.59712  2.45038  2.31414  2.31414  2.07065  1.96219
            1.86209  1.76934  1.68382  1.68382  1.53230  1.46558
            1.40439  1.34837  1.29722  1.29722  1.20832  1.17001
            1.13548  1.10451  1.07689  1.07689  1.03084  1.01203
            0.99580  0.98199  0.97036  0.97036  0.95301  0.94702
            0.94266  0.93981  0.93837  0.93837  0.93926  0.94139
            0.94451  0.94855  0.95341  0.95341  0.96525  0.97210
            0.97946  0.98728  0.99551  0.99551  1.01294  1.02205
            1.03136  1.04084

```

C -----

```

fc854 deuteron image at IL1 -- d's are the largest fraction of other stuff
fmesh854:d geom=rec origin=-7 -7 +1.0
imesh 7 iints 1400
jmesh 7 jints 1400      kmesh  +1.2  out=cf
DE854 LIN  5.06578  5.52427  6.02426  6.56950  7.16409  7.81250
            8.51959  9.29068  10.13160  11.04850  12.04850  13.13900
            14.32820  15.62500  17.03920  18.58140  20.26310  22.09710
            24.09700  26.27800  28.65640  31.25000  34.07840  37.16270
            40.52620  44.19420  48.19410  52.55600  57.31280  62.50000
            68.15670  74.32540  81.05250  88.38830  96.38820  105.11200
            114.62600  125.00000  136.31300  148.65100  162.10500  176.77699
            192.77600  210.22400  229.25101  250.00000  272.62701  297.30200
            324.20999  353.55301  385.55301  420.44800  458.50201  500.00000
            545.25403  594.60400  648.41998  707.10699  771.10498  840.89600
            917.00403  1000.00000
DF854 LIN  46.99316  43.84974  40.86316  40.86316  35.35503  32.83821 $ ratio of deuteron dE/dx
            30.45042  28.19230  26.07328  26.07328  23.06054  21.76551 $ to proton dE/dx at 1-GeV
            20.52985  19.35507  18.23888  18.23888  16.17406  15.21982

```

14.32294	13.46847	12.66044	12.66044	11.17413	10.49369
9.85235	9.24588	8.67708	8.67708	7.63658	7.16322
6.71806	6.30098	5.90950	5.90950	5.19951	4.87786
4.57721	4.29610	4.03353	4.03353	3.55937	3.34606
3.14718	2.96202	2.78962	2.78962	2.48081	2.34240
2.21404	2.09500	1.98478	1.98478	1.78873	1.70176
1.62150	1.54761	1.47970	1.47970	1.36034	1.30822
1.26072	1.21756				

C

fc954 triton image at IL1

fmesh954:t geom=rec origin=-7 -7 +1.0

imesh 7 iints 1400

jmesh 7 jints 1400 kmesh +1.2 out=cf

DE954 LIN	5.06578	5.52427	6.02426	6.56950	7.16409	7.81250
	8.51959	9.29068	10.13160	11.04850	12.04850	13.13900
	14.32820	15.62500	17.03920	18.58140	20.26310	22.09710
	24.09700	26.27800	28.65640	31.25000	34.07840	37.16270
	40.52620	44.19420	48.19410	52.55600	57.31280	62.50000
	68.15670	74.32540	81.05250	88.38830	96.38820	105.11200
	114.62600	125.00000	136.31300	148.65100	162.10500	176.77699
	192.77600	210.22400	229.25101	250.00000	272.62701	297.30200
	324.20999	353.55301	385.55301	420.44800	458.50201	500.00000
	545.25403	594.60400	648.41998	707.10699	771.10498	840.89600
	917.00403	1000.00000				

DF954 LIN	63.82817	59.91015	56.16025	56.16025	49.15790	45.91025	\$ ratio of triton dE/dx
	42.82045	39.88614	37.11004	37.11004	32.01544	29.66841	\$ to proton dE/dx at 1-GeV
	27.46039	25.38572	23.95152	23.95152	21.33982	20.12637	
	18.97208	17.87300	16.83272	16.83272	14.91396	14.02916	
	13.18993	12.39757	11.64733	11.64733	10.27243	9.64296	
	9.04943	8.49191	7.96623	7.96623	7.00925	6.57388	
	6.16580	5.78267	5.42411	5.42411	4.77385	4.47999	
	4.20520	3.94859	3.70890	3.70890	3.27715	3.08300	
	2.90226	2.73404	2.57816	2.57816	2.29787	2.17273	
	2.05674	1.94937	1.85027	1.85027	1.67385	1.59580	
	1.52399	1.45801					

C

fc1054 3He image at IL1

fmesh1054:s geom=rec origin=-7 -7 +1.0

imesh 7 iints 1400

jmesh 7 jints 1400 kmesh +1.2 out=cf

DE1054 LIN	5.06578	5.52427	6.02426	6.56950	7.16409	7.81250
	8.51959	9.29068	10.13160	11.04850	12.04850	13.13900
	14.32820	15.62500	17.03920	18.58140	20.26310	22.09710
	24.09700	26.27800	28.65640	31.25000	34.07840	37.16270
	40.52620	44.19420	48.19410	52.55600	57.31280	62.50000
	68.15670	74.32540	81.05250	88.38830	96.38820	105.11200
	114.62600	125.00000	136.31300	148.65100	162.10500	176.77699
	192.77600	210.22400	229.25101	250.00000	272.62701	297.30200
	324.20999	353.55301	385.55301	420.44800	458.50201	500.00000
	545.25403	594.60400	648.41998	707.10699	771.10498	840.89600
	917.00403	1000.00000				

DF1054 LIN	251.35355	236.69599	222.48483	222.48483	195.55695	182.91138	\$ ratio of helion dE/dx
	170.79847	159.23402	148.24679	148.24679	127.99319	118.63409	\$ to proton dE/dx at 1-GeV
	109.81699	101.52535	95.79416	95.79416	85.34892	80.49541	
	75.87840	71.48250	67.32202	67.32202	59.64778	56.10900	
	52.75274	49.58344	46.58300	46.58300	41.08420	38.56652	
	36.19267	33.96295	31.86046	31.86046	28.03308	26.29187	
	24.65978	23.12746	21.69341	21.69341	19.09277	17.91749	
	16.81848	15.79222	14.83359	14.83359	13.10683	12.33043	
	11.60751	10.93476	10.31132	10.31132	9.19032	8.68987	
	8.22594	7.79659	7.40023	7.40023	6.69472	6.38256	
	6.09534	5.83149					

C

fc1154 alpha image at IL1

fmesh1154:a geom=rec origin=-7 -7 +1.0

imesh 7 iints 1400

jmesh 7 jints 1400 kmesh +1.2 out=cf

DE1154 LIN	5.06578	5.52427	6.02426	6.56950	7.16409	7.81250
	8.51959	9.29068	10.13160	11.04850	12.04850	13.13900
	14.32820	15.62500	17.03920	18.58140	20.26310	22.09710

	24.09700	26.27800	28.65640	31.25000	34.07840	37.16270	
	40.52620	44.19420	48.19410	52.55600	57.31280	62.50000	
	68.15670	74.32540	81.05250	88.38830	96.38820	105.11200	
	114.62600	125.00000	136.31300	148.65100	162.10500	176.77699	
	192.77600	210.22400	229.25101	250.00000	272.62701	297.30200	
	324.20999	353.55301	385.55301	420.44800	458.50201	500.00000	
	545.25403	594.60400	648.41998	707.10699	771.10498	840.89600	
	917.00403	1000.00000					
DF1154 LIN	301.14149	285.98364	270.49441	270.49441	240.57549	226.23997	\$ ratio of alpha dE/dx values
	212.38032	199.03174	186.25032	186.25032	162.27752	151.12927	\$ to proton dE/dx at 1-GeV
	140.61071	130.57880	121.09534	121.09534	103.69260	97.26703	
	91.85572	86.69168	81.76917	81.76917	72.63794	68.41291	
	64.41078	60.62861	57.03621	57.03621	50.41296	47.37011	
	44.49215	41.78218	39.22719	39.22719	34.54728	32.40993	
	30.40391	28.51857	26.74653	26.74653	23.52734	22.06799	
	20.70093	19.42070	18.22400	18.22400	16.05998	15.08374	
	14.17299	13.32413	12.53271	12.53271	11.10994	10.47421	
	9.88132	9.33070	8.82005	8.82005	7.90815	7.50345	
	7.12849	6.78267					

c -----
c ----- | ----- | ----- | ----- | ----- | ----- | ----- |